HALMSTAD UNIVERSITY

Master's Programme in Microelectronics and Photonics, 60 credits

MASTER THESIS

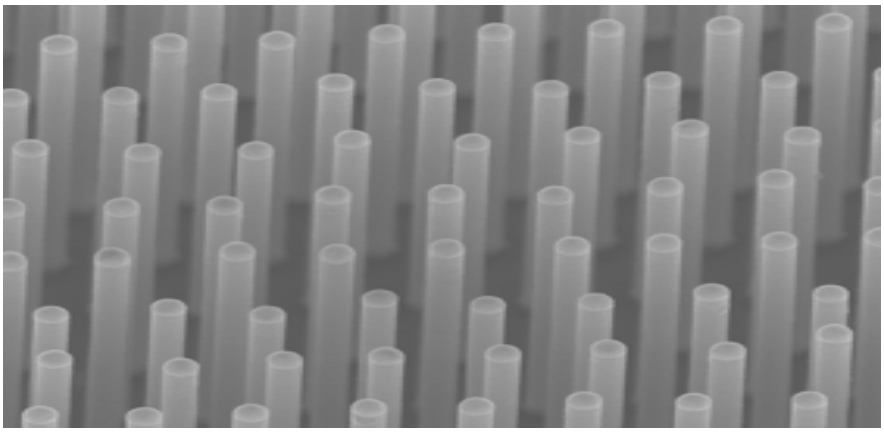

Electrical and Optical Characterization of InAsP/InP Nanowire-Based Avalanche Photodetectors

Praveen Kumar Singaravelu, Mohammad Tawhidul Alam

Solid state physics, 15 credits

Halmstad 2015-06-09

Electrical and Optical Characterization of InAsP/InP Nanowire-Based Avalanche Photodetectors

Master's Thesis in Microelectronics and Photonics

School of Information Technology
Halmstad University
Box 823, S-301 18 Halmstad
Sweden

Description of cover page image: - SEM image of InP nanowires grown at Lund University

Acknowledgement

We are grateful to our supervisor Håkan Pettersson for his warm guidance and support throughout this thesis. He took special care in this project and helped us in all kinds of issues.

We specially thank PhD student Mohammed Karimi for teaching us basic knowledge of this research field and helping us in laboratory.

We would like to thank Lund University and PhD student Vishal Jain for fabricating the devices.

Our families have been of great support, emotionally and materially, during the whole master program and especially during the period when we were focusing on writing this thesis.

Finally, we have to thank our friends for helping us in all aspects and encouraging us.

ABSTRACT

The availability of new manufacturing methodology in solid state physics makes it possible to grow nano-photonic devices for better performance and unique properties. In this thesis work, we use *I-V* and *FTIR* spectroscopy to study the electrical and optical properties of *InAsP/InP* nanowire-based array avalanche photodetectors for near infrared applications. Measurements are performed at 300K and 5K for different applied biases under darkness and illumination conditions. *I-V* curves are plotted to understand the charge carrier transport in nanowire photodetectors and also to improve the device fabrication. *I-V* characteristics display non-optimal diode properties with large dark leakage currents. From spectrally resolved photocurrent measurements, peaks appear at photon energies of 1.34eV and 1.4eV respectively, corresponding to the bandgap of zinc blende (*ZB*) and wurtzite (*WZ*) *InP*. An additional photocurrent peak at 1.25eV agrees with the bandgap of the included *InAsP* segments. The Schottky-like contacts present at the top of the nanowires most likely generate additional photocurrent at higher photon energies. No breakdown effect is observed for the array devices. Complementary single-nanowire devices indicate an avalanche breakdown effect at V_R=-35V.

Abbreviations

q: Charge of electron

eV: Electron volt

μ_e: Mobility of electron

E_g: Bandgap of semiconductor in eV

E_{ph}: Energy of photon in eV

V_F: Forward bias

V_R: Reverse bias

V_{BD}: Breakdown voltage

E_c: Energy level of conduction band in eV

E_v: Energy level of valence band in eV

p-n: Adjacent regions of acceptors and donors

i: Intrinsic layer

InAsP: Indium arsenide phosphide

InP: Indium phosphide

Au**:** Gold

MOVPE: Metal organic vapor phase epitaxy

VPE: Vapor phase epitaxy

CVD**:** Chemical vapor deposition

NWs: Nanowires

IR: Infrared radiation

NIR: Near-wavelength infrared radiation

MIR: Mid-wavelength infrared radiation

LIR: Long-wavelength infrared radiation

FTIR: Fourier transform infrared spectroscopy

SEM: Scanning electron microscope

APDs: Avalanche photodiodes

CCD: Charge coupled device

SNR: Signal-to-noise ratio

List of Figures

List of Graphs

Table of contents

1 INTRODUCTION

A large part of the electromagnetic radiation from the sun is absorbed by the earth and re-emitted as infrared radiation in the form of heat to provide life for all living species. Infrared radiation has longer wavelengths than visible light. Infrared radiation is further classified into near-infrared, mid-wavelength infrared and long-wavelength infrared depending upon their wavelength range. It is very important to detect these portions of the electromagnetic spectrum for many different applications.

One of the most important applications of near-infrared radiation is in optical communication (1.3-1.55 μm). Other applications can be found in pharmaceutical and medical diagnostics. The detection of near-infrared radiation is also important in astronomical spectroscopy. In astronomical spectroscopy, the near-infrared spectrum is used to find e.g. the composition of gases present in the atmosphere of stars in outer space.

In this thesis work, novel p^+-i-n^+ *InP/InAsP* double heterostructure avalanche photodetectors is designed for the near-infrared region. The electrical and optical properties of the photodetectors are studied with the help of Fourier transform infrared spectroscopy and *I-V* measurements.

1.1 Research Aim

The aim of this project is to investigate optoelectronic properties of nanowire-based avalanche photodetectors with separate absorption and multiplication regions. More specifically the research tasks are:

To measure and analyse the current-voltage characteristics of *InAsP/InP* nanowire-based avalanche photodetectors under darkness and illumination conditions. To obtain spectrally resolved photocurrent data for both forward bias and reverse bias conditions. And also, study the breakdown mechanisms of nanowire based photodetectors.

1.2 Semiconductors

In semiconductor industry, the directions of study were changed in the 1970's and 1980's due to new emerging technologies. The dual nature of electrons (i.e. particle and wave) led to the discovery of new physical phenomena and to a paradigm shift in semiconductor device technology. In the 1970's the first high-quality quantum well based heterostructure materials were developed by molecular beam epitaxy (*MBE*) which led to the development of new devices such as resonant tunneling diodes and modulation-doped field effect transistors [3]. In heterostructure physics, two crucial parameters are the lattice matching of the different materials and the corresponding bandgaps.

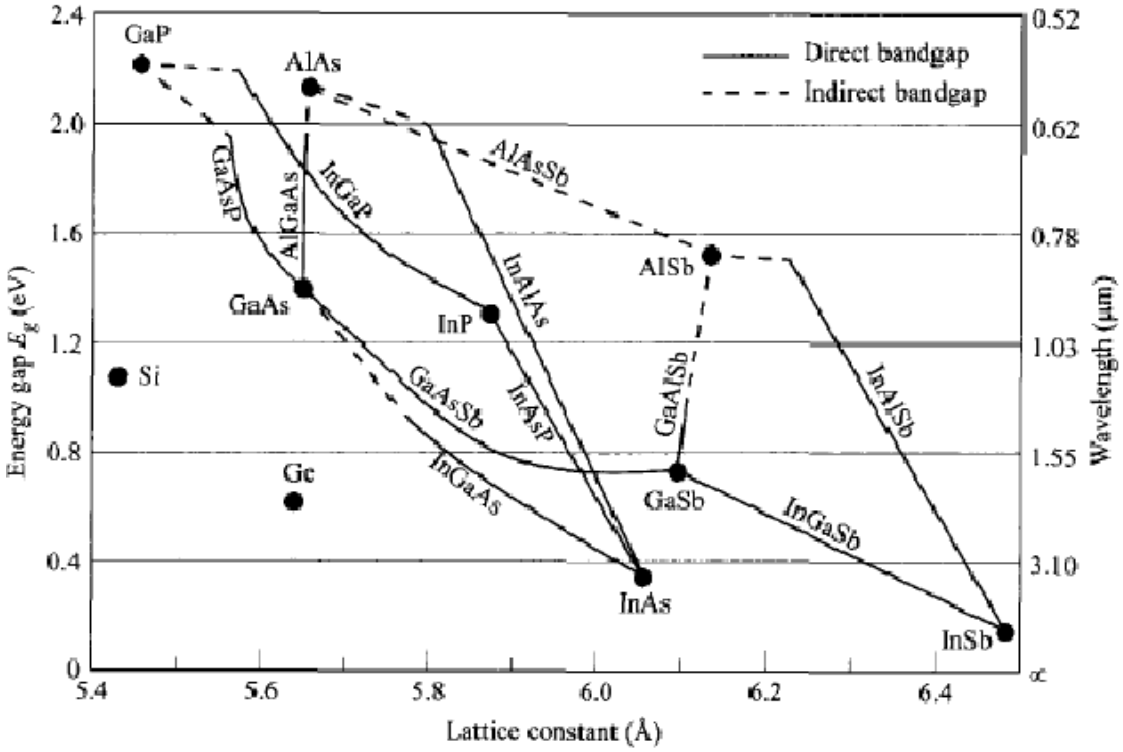

Figure 1.1: Relationship between bandgap and lattice constant of different heterostructures [3]

1.3 Heterojunction in nanostructures

A heterostructure junction is formed between two different semiconductor materials. The difference in bandgap between two semiconductors provides a unique property to tailor the energy landscape of the charge carriers (i.e. electrons and holes). This makes heterojunctions widely used in many device applications such as hetero-junction bipolar transistors and lasers. The difference in lattice constant between two different semiconductors creates physical defect states at the interface between them. It limits the possible combinations of materials used for the formation of heterojunctions.

Particularly interesting heterojunction devices are made from materials with almost the same lattice constant, but with different bandgap energy *Eg*. The heterostructure InAsP/InP is a good example as shown in figure 1.1. These combinations of materials have direct bandgap which makes them suitable for optoelectronic devices [3]. The band alignment in heterojunctions is explained by the Anderson rule or electron affinity rule [8]. Depending upon the alignment of energy bands with reference to the vacuum level, heterostructures are classified into three types is shown below.

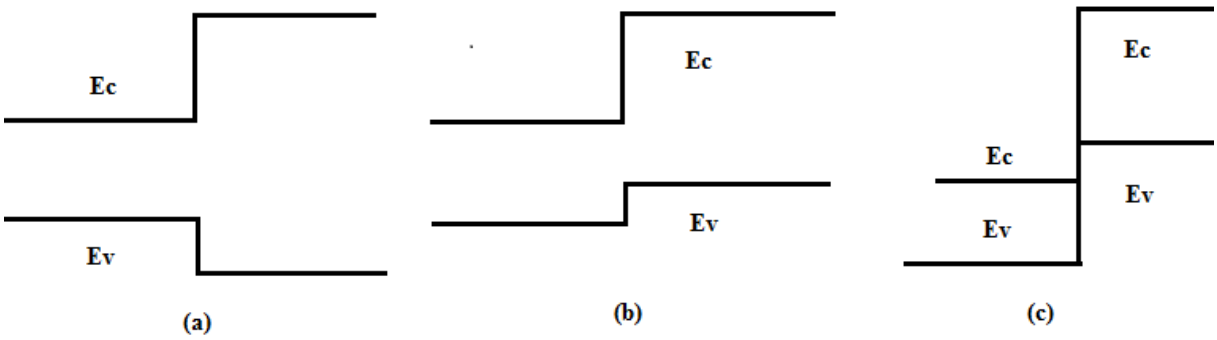

Figure 1.2: (a) Straddling-band alignment (b) Staggered-band alignment (c) Broken bandgap

i. Type I or Straddling band alignment

In straddling band alignment, one of the semiconductors have both lower conduction band E_c and higher valence band E_v relative to the other semiconductor as seen in figure 1.2-a [7].

ii. Type II or Staggered band alignment

In staggered band alignment, the valence band or conduction band of the low-bandgap semiconductor is lower the corresponding band of the high-bandgap semiconductor as seen in figure 1.2-b [7].

iii. Type III or Broken bandgap

The type III or broken band alignment is a rare case of type II band alignment. In this case, the band edges of the low-bandgap material are completely displaced relative the high-band gap material as seen in figure 1.2-c [7].

1.4 Quantum wells and superlattice

A quantum well is a thin semiconductor layer with a thickness of the order of a few nanometers with small bandgap sandwiched in between thick barriers of large bandgap material. The band offsets ΔE_c and ΔE_v form barriers for the charge carriers. For example: a thin layer of GaAs forms a quantum well in AlGaAs by forming a type-I band alignment [3]. The quantum well is confined in one dimension (the growth direction) whereas the charge carriers are allowed to move freely in other two-dimension y and z.

The confinement of charge carriers inside a well makes the charge carriers behave as "waves". The one- dimensional equation for infinite wells, describes the wave nature of charge particles inside a well [5].

$$\Psi(x) = A^{*}\sin\left(\frac{i\pi x}{Lx}\right) \quad (1)$$

Where 'i' is an integer and L_x is the well width.

The confinement of charge carriers inside a well creates a quantization of the electronic structure described by the equation:

$$E_i = \frac{\hbar^2 \pi^2 i^2}{2m^* L_x^2} \quad (2)$$

The conduction and valence bands are divided into inter-sub bands. The energy structure is only confined in one direction. In multiple quantum wells, the quantum wells are typically separated from each other by thick barriers. The electrons cannot tunnel through the thick barriers. Once the thick barriers are replaced by thin barriers, the electrons start to tunnel through the barriers forming mini-bands can be seen in figure 1.3. There are no more discrete energy levels inside the quantum wells. Such a structure is referred to as a superlattice.

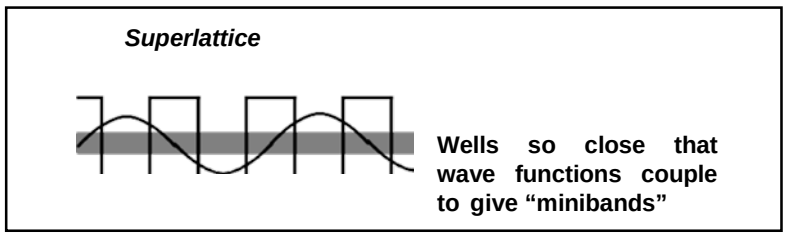

Figure 1.3: Structure of multiple quantum wells and superlattice [7]

2 Backgrounds

2.1 Photodetectors

Photodetectors are devices which are sensitive to incoming electromagnetic radiation. There are different types of photodetectors, some being mentioned below:

i. Photo diodes
ii. Photo transistors
iii. Photo resistors
iv. Charge-Coupled Devices (CCDs)

2.2 Photodiodes

A photodiode consists of a junction between electron-rich (n-type) and electron-poor (p-type) regions. A depletion layer (W) with few free charge carriers is formed around the physical interface between the two regions resulting in a large built-in electric field. When incident photons of energy ($h\nu$) equal to or larger than the bandgap of the semiconductor material (Eg) are absorbed in the depletion region, electron-hole pairs are generated and subsequently separated by the built-in electric field. These electrons and holes generate a photocurrent in the external circuit [1].

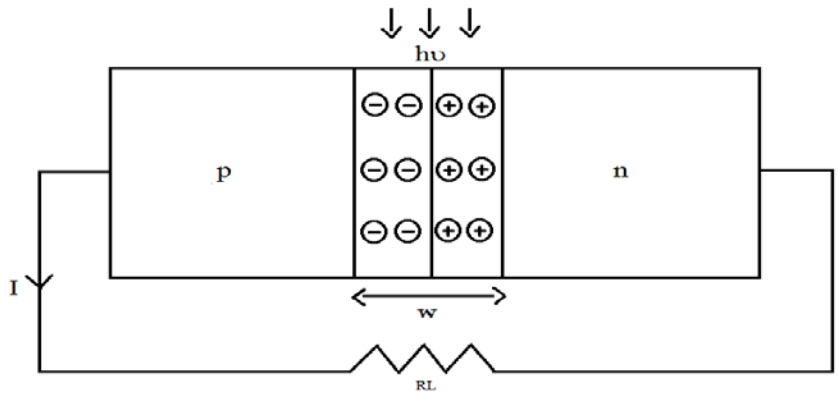

Figure 2.1: Design of p-n photodiode with incoming photons

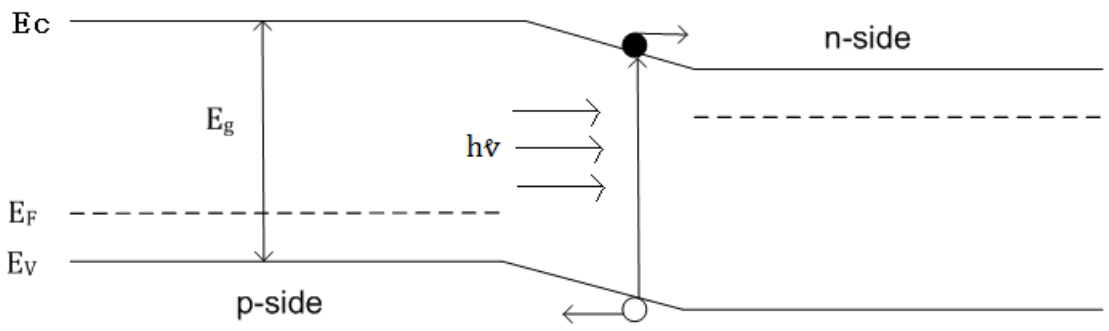

Figure 2.2: Energy-band diagram of p-n photodiode under illumination condition

2.3 Types of Photodiodes

The most common types of photodiodes are:

i. p-n photodiodes
ii. p-i-n photodiodes
iii. Metal-Semiconductor photodiodes (Schottky diodes)

i. p-n photodiodes

It is a simple geometry photodiode of which one side of the semiconductor is p-doped and another side is n-doped. A junction where electron-hole pairs are photo-generated is formed between two oppositely charged regions. This type of photodiode is normally operated under reverse bias conditions to yield high quantum efficiency, but meanwhile response speed becomes slower. Under reverse bias conditions, controlled breakdown mechanisms can enhance both quantum efficiency and response speed.

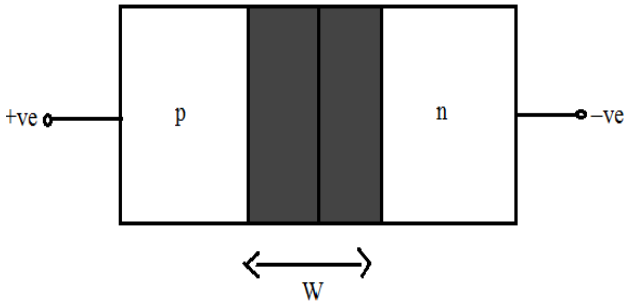

Figure 2.3: Simple design of p-n photodiode

ii. p-i-n photodiodes

An intrinsic (i-) layer is formed between the n- and p- regions to achieve high quantum efficiency. The incoming photons are absorbed in this region. Due to the large absorption volume of the intrinsic region, it enables higher absorption of photons. These photons are converted into large number of photo-generated charge carriers to achieve high quantum efficiency.

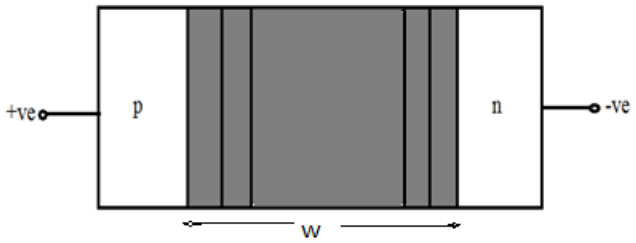

Figure 2.4: Simple design of p-i-n photodiode

iii. Metal – Semiconductor diodes (or) Schottky diodes

A thin layer of metal is deposited on a semiconductor surface to form a shallow junction. Usually n-type semiconductors are preferred for this type of photodiode due to high drift velocity of electrons. This type of detector is frequently used to detect short wavelength radiation due to the surface-near electric field. Schottky diodes are inherently fast due to their unipolar character.

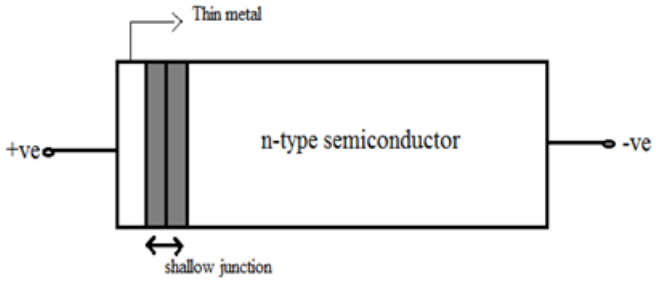

Figure 2.5: Simple design of metal-semiconductor photodiode (or) Schottky diode

2.4 Breakdown Mechanisms

Breakdown mechanisms are the reverse bias characteristics of a photodiode. During lower reverse bias condition, a small current flow corresponds to leakage current. Beyond a critical reverse bias voltage the current increases drastically due to two different possible mechanisms: Zener and avalanche breakdown [1].

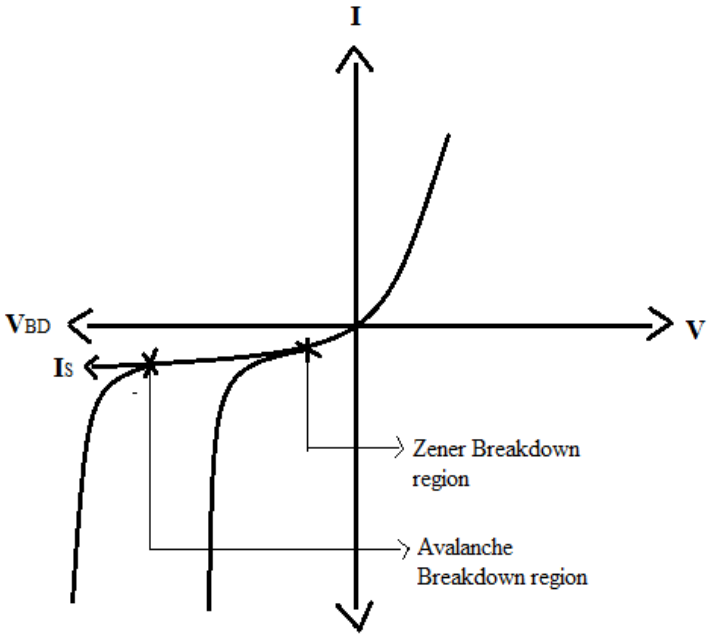

Figure 2.6: Graph shows different breakdown regions

2.4.1) Zener Breakdown

The physical mechanism for Zener breakdown is tunneling through the bandgap barrier (Fig. 2.8a). Typical breakdown voltages $V_R = V_{BD} \leq \frac{4Eg}{q}$. The Zener breakdown voltage (V_{BD}) decreases with increasing temperature due to the decrease of the bandgap.

2.4.2) Avalanche Breakdown

If the observed breakdown voltage $V_R = V_{BD} \geq \frac{6Eg}{q}$, the most likely breakdown mechanism is the avalanche effect. Photo-generated carriers gain sufficient kinetic energy to break crystal bonds on impact with lattice atoms. Repeated collision processes rapidly increase the number of electron-hole pairs (avalanche effect). The avalanche breakdown voltage (V_{BD}) increases with temperature due to the decrease in mobility at elevated temperature. The decrease in mobility with increasing temperature is the result of increased phonon (lattice) lattice scattering dominating over impurity scattering. The influence of the two different scattering mechanisms on the mobility results in an effective mobility given by [1]:

$$\frac{1}{\mu e} = \frac{1}{\mu lattice} + \frac{1}{\mu impurity} \tag{3}$$

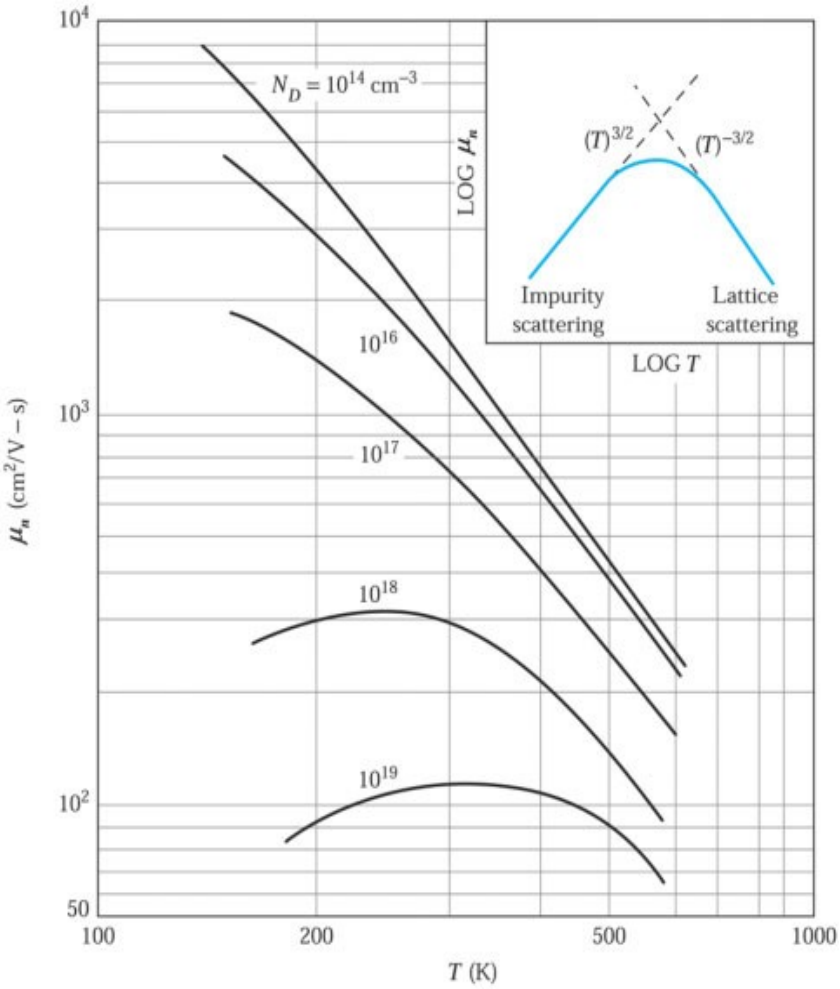

Figure 2.7: Graph shows the relation between electron mobility and temperature as a function of doping profile [1]

2.5 Impact Ionization Process (Avalanche Breakdown)

When the electric field in a photodiode is increased above the critical field for avalanche breakdown, the free electrons and holes (Fig 2.8b) are accelerated with high saturation velocity (V_s) and collide with the atoms in the crystal lattice. Most of the kinetic energy of a charge carrier is spent in breaking a bond in the crystal lattice generating a new electron-hole pair (denoted by 2 and 2′). The new electron and hole are again accelerated by the applied electric field and collide with the neighboring crystal lattice atoms, which results in further generation of electron-hole pairs (denoted by 3 and 3′) and so on. The generation of new charge carriers by applying large electric field in a semiconductor material is called avalanche process or impact ionization process [11].

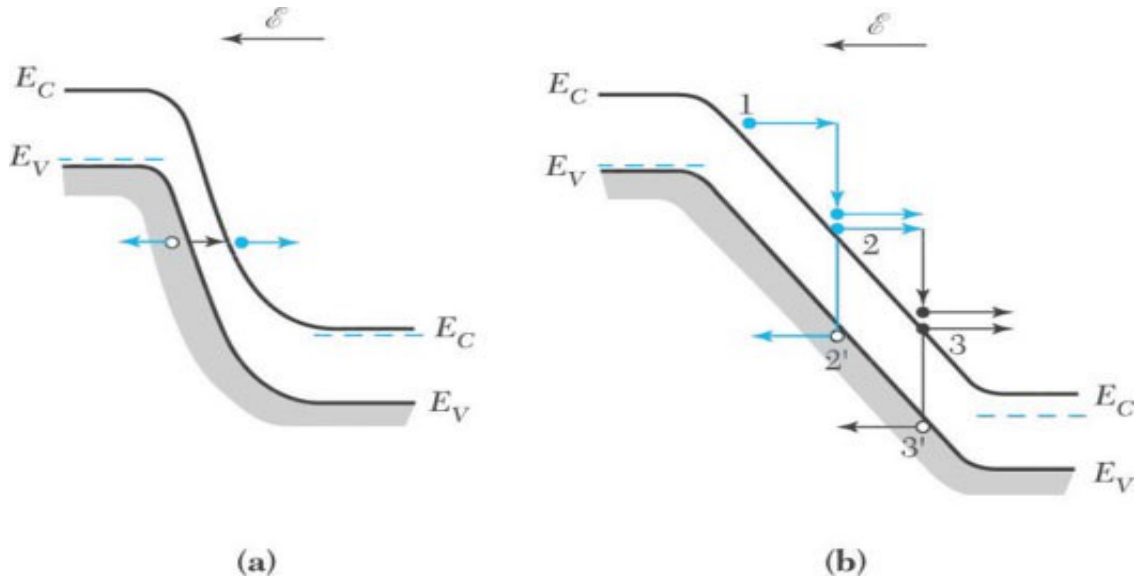

Figure 2.8: a) Zener tunneling b) Avalanche process [1]

2.5.1) Gain and Noise

Gain

The gain in an avalanche process depends on the multiplication factor or ionization rate. The electron ionization rate is denoted by α and hole ionization rate is denoted by β (eqn. 4). The ionization rate in a photodiode depends on the electric field in the avalanche region (i.e. applying reverse bias voltage) and also on the number of charge carriers available in this region (i.e. doping concentration). The gain in APDs furthermore depends on the temperature (i.e. the thermal energy $\frac{kT}{q}$) [6].

$$\text{K (ionization rate)} = \frac{\beta\ (hole\ ionization\ rate)}{\alpha\ (electron\ ionization\ rate)} \qquad (4)$$

Noise

The noise in APDs is explained in terms of signal-to-noise ratio (SNR). The signal-to-noise ratio is generally defined as the comparative level of a desired signal to the background noise. In APDs there are two main types of noise shown in eqn. 5 below [6].

$$\text{SNR} = \frac{I_L^2 M^2}{2q(I_L+I_{dg})BM^2F+2qI_{ds}+\frac{4kTB}{R_L}} \quad (5)$$

Where,

I_L^2- Photocurrent generated by a photodiode

M^2- Multiplication factor

q- Charge of an electron

I_{dg}- Dark current flowing in the avalanche region

B – Bandwidth of a detector

F- Fano noise

I_{ds}- Dark current flowing outside of the avalanche region

K- Boltzmann constant

T- Temperature in Kelvin

R_L- Load resistances connected series to a photodiode

In eqn. (5) the component $2q(I_L + I_{dg})BM^2F + 2qI_{ds}$ is termed shot noise and other part $\frac{4kTB}{RL}$ is termed thermal noise. The shot noise has two components: the noise due to the surface dark current (I_{ds}) and generated photocurrent (I_L). The surface dark current (I_{ds}) noise does not depend on the avalanche gain, because it is a tiny current flowing on the surface of a photodiode (not in the avalanche region), whereas the generated photocurrent (I_L) flows in the avalanche region with a noise amplified by an avalanche gain (M). Due to the strong reverse bias condition, some of the dark current also flows in the avalanche region and is thus multiplied by an avalanche gain. It seems the noise in APDs strongly depends upon the avalanche gain (M) mechanism. In addition, the spectral dependence of the gain includes the bandwidth (B) of a detector in the noise equation.

Thermal noise

The source of thermal noise is the thermal energy of electrons. It can be reduced by adding a large value series resistance (R_L). Higher values of the load resistance completely reduce the thermal noise, but simultaneously reduce the response speed of the photodiode. There is thus a tradeoff between thermal noise and response speed. In case of APDs the response speed increased by increasing the avalanche gain until the shot noise equals the thermal noise.

In addition to all the noise sources discussed above, the Fano noise should also be added due to the random fluctuations of electric charges in the avalanche region. However, it is typically much smaller than the other noises.

2.5.2) Temperature and Spectral dependence

Temperature

The gain characteristics of APDs are temperature dependent. The rise in temperature vibrates the crystal lattice strongly, which leads to collisions of free carriers with phonons preventing the carriers from reaching sufficiently high energy to trigger ionization processes.

Spectrum

The gain characteristic of APDs is dependent on the wavelength (photon energy (E_{ph})) of incident light (hν). For an optical detector, only photons of certain energy can be absorbed to create photo-generated charge carriers. Those charge carriers trigger the avalanche process. This means that the gain of APDs is indirectly dependent upon the wavelength of incident light, which we can see clearly in the below equation.

$$\lambda\ (\mu m) = \frac{1.24}{Eg(ev)} \qquad (6)$$

Where,

λ - Wavelength of incident light in μm

E_g - Bandgap of a semiconductor in electron volts

2.5.3) Disadvantages and Applications of APDs

Disadvantages

It may require much higher operating voltage. It produces much higher noise compared to p-i-n photodiodes. The output is not linear because of avalanche process.

Applications

In optical communication, due to extremely large band width. APDs are being used in many space research applications due to higher sensitivity. When APDs are operated in Geiger mode, they can be used as photon counting devices. APDs are also used in particle physics and positron emission tomography.

2.6 Current-Voltage Relations

To understand the device functionality, it is very important to study the *I-V* performance. The current-voltage (I-V) characteristics of different photodetector devices have been studied in this thesis work. All the investigated samples are based on a p-n junction (diode) design as previously explained

The well-known diode equation is given by:

$$I = I_o \left(e^{qV/\eta kT} - 1\right) \quad (7)$$

Here η is the ideality factor which indicates the dominant transport mechanism. The standard procedure to extract the ideality factor is to plot lnI vs applied bias V. The ideality factor is then deduced from the slope while the intercept gives the lnI_o value.

$$I = I_o\, e^{\frac{qV}{\eta kT}} \quad (8)$$

$$\mathbf{lnI} = lnI_o + \frac{q}{\eta kT}.\,\mathbf{V} \quad (9)$$

From this the slope of LnI vs V is given by:

$$\text{Slope} = \frac{q}{\eta kT}$$

$$\Rightarrow \boldsymbol{\eta} = \frac{q}{slope * kT}$$

Where,

η = 1 indicates that diffusion current is dominating

η = 2 indicates that recombination current is dominating

1 < η < 2 indicates that both diffusion and recombination currents are present

During illumination the diode equation is modified due to the generated photocurrent I_L.

$$I = I_o \left(e^{\frac{qV}{\eta kT}} - 1\right) - I_L \quad (10)$$

2.7 Wavelength-Photonenergy Relations

The spectrally resolved photocurrent was investigated using Fourier transform spectroscopy as previously described. The obtained spectral data are in units of inverse cm. The data are converted into wavelength in micrometer using the expression below:

$$\text{Wavelength } (\mu\text{m}) = \frac{10^4}{wavenumber(cm^{-1})} \quad (11)$$

The obtained photocurrent spectra can also be converted to units of photon energy using the formula:

$$E_{ph} = \frac{hc}{\lambda} \quad (12)$$

Where,

h is Planck's constant ≈ 6.626 * 10^{-34} Js

c is the speed of light ≈ 3 * 10^8 m/s

λ is the wavelength of the incoming electromagnetic radiation.

The conversion of wavelength in micrometer to photon energy in electron volt is done by the simple expression below:

$$E_{ph}\ (\text{eV}) = \frac{1.24}{\lambda(\mu m)} \quad (13)$$

Where,

E_{ph} is the photon energy in electron volt

λ is the wavelength in micrometer

3 Device Descriptions

3.1) Nanowires

Nanowires (NWs) are needle-like semiconductor materials with diameter and length in the range of some tens of nm and a few μm, respectively. The flow of charge carriers in ultra-thin NWs is only allowed in one dimension and confined in the other two dimensions, which gives rise to quantum mechanical effects such as quantum tunneling in the electron transport phenomena [9].

3.1.1) Surface effects in Nanowires

The conductivity of NWs is dependent upon the surface structure. If there are any atoms on a surface of nanowires which are not bounded to the neighboring atoms; those unbounded atoms arises a physical defect states in a nanowire. Surface atoms of NWs produce surface states which might lead to high surface dark currents. Methods to circumvent these problems include growth of a thin protective semiconductor shell or other surface passivation.

3.1.2) Uses of Nanowires

The applications of NWs include e.g. nano-electronics (transistors and p-n junctions), nano-photonics (LEDs, photodetectors, lasers and solar cells) and life science applications.

3.2) Fabrication of Nanowires

To synthesize nanowires there are two approach:

i) Top – Down

ii) Bottom - Up

i) Top-Down

The basic idea of the top-down approach is to back etch a semiconductor substrate using a pattern defined by lithography. There is considerably amount of material wasted during the back etching process. Less flexibility in choice of materials for fabrication of heterostructures.

ii) Bottom-Up

The bottom-up approach is opposite to the top-down approach. In this approach we selectively grow NWs from some seed catalyst particles defined on the substrate surface. Less materials waste. Large flexibility in materials choice. The devices studied in this thesis work are synthesized by Metal Organic Vapor Phase Epitaxy (*MOVPE*).

3.2.1) Metal Organic Vapor Phase Epitaxy (*MOVPE*)

In MOVPE, the substrate is placed in a special growth reactor. The reactor chamber is made from materials like quartz which is able to withstand the high temperatures during growth. A carrier gas e.g. nitrogen is used to transfer precursor gases inside the reactor. Usually, gold (Au) particles are deposited on the wafer for NW growth prior to

loading the wafer into the reactor. The substrate with Au particles is gradually heated forming a super saturated Au-substrate alloy. Now the precursor gases are introduced into the reactor chamber. Nanowires start growing at the interface between seed particle and substrate as seen in figure 3.1. The diameter of the grown NWs is roughly equal to the seed particle diameter. The growth rate of NWs is controlled by controlling the flow of precursor gases and temperature of the reactor [12].

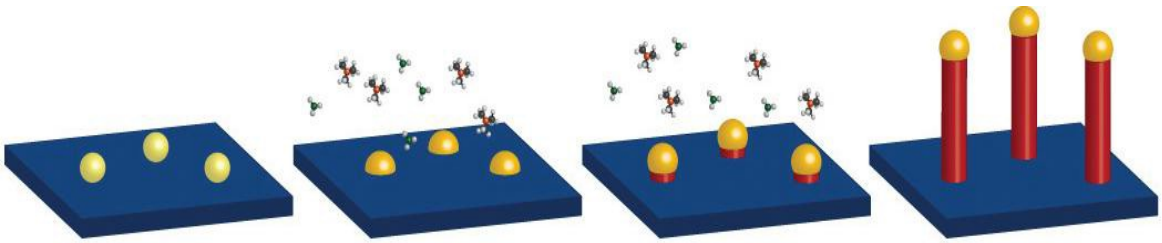

Figure 3.1: Growth of nanowires by *MOVPE* [12]

3.3) Device Structure

In our APD devices, the NWs are made of heterostructures of indium arsenide phosphide (*InAsP*) and indium phosphide (*InP*) grown on p^+ *InP* substrates. The various NW segments have different dopants as seen in figure 3.2. The top segments of the NWs are heavily n-doped for making good contact to the transparent ITO layer. The APDs have separate absorption and multiplication regions as seen in figure 3.2. The n-InAsP absorption region is spectrally tuned to the wavelength region to be detected, while the multiplication region consists of an *InP* p-n junction with high electric field. The silicon dioxide (SiO_2) layer is deposited on the NW side walls and in between the NWs to electrically isolate the NWs from each other. Indium tin oxide layer is used to connect the NWs in parallel [10].

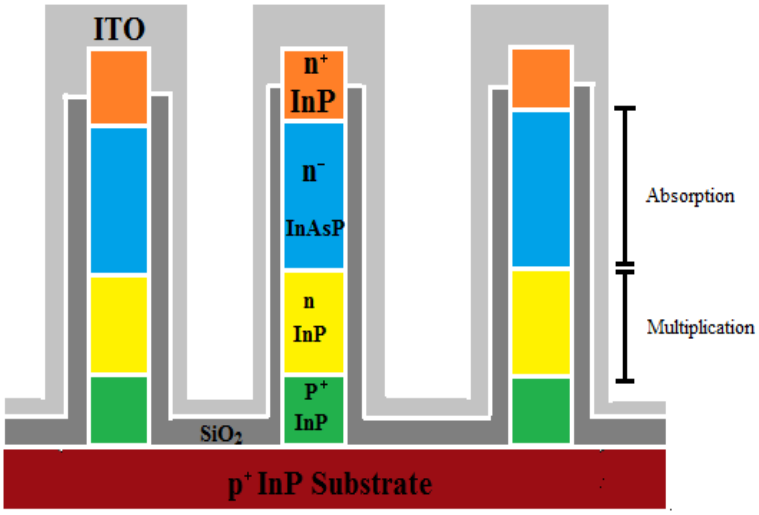

Figure 3.2: Device structure

Planar Structure

The planar structure of a device is shown below with separate absorption and multiplication region. The photo-generated charge carrier is generated in the absorption region and enters to the avalanche region. Due to strong reverse biased condition; this region has high electric field strength as seen in figure 3.4.

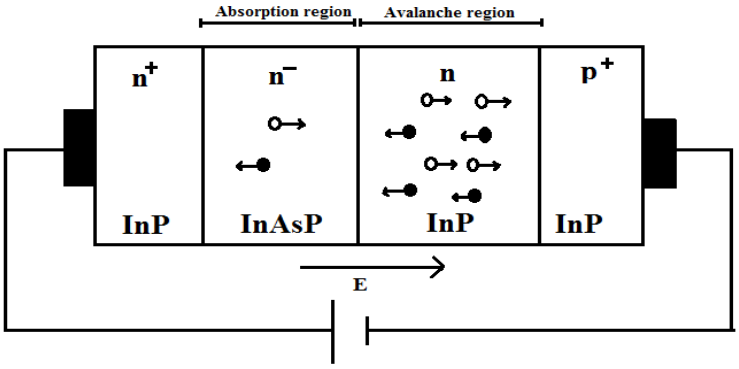

Figure 3.3: Planar structure of device

Bandgap and Electric field distribution

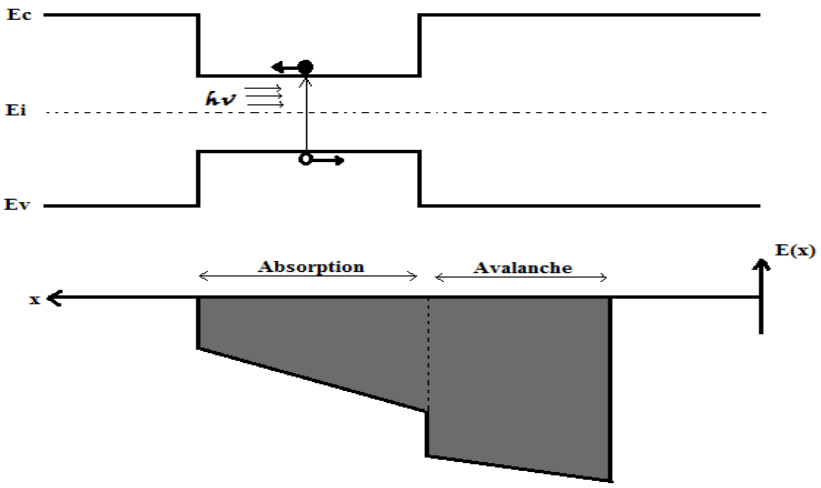

Figure 3.4: Band gap and electric field distribution

4 Laboratory Setup

For the characterization of the NW APDs we used a Fourier Transform Infrared Spectrometer combined with a close-cycle helium cryostat, a Keithley 428 current amplifier and a Keithley 6430 source meter.

4.1) Fourier Transform Infrared Spectrometer (*FTIR*)

Light Sources

There are different types of built-in light sources that can be used in the spectrometer depending on the desired spectral range. The Vertex 80v spectrometer is equipped with a quartz-lamp for NIR light source.

Beam splitter

Different types of beam splitters are used in the spectrometer depending on the spectral range. The CaF_2 (Spectral range- 15,500-1,200 cm^{-1}) beam splitter was used during our measurements.

Laser

The Vertex 80v spectrometer is equipped with a standard He-Ne laser that emits wavelength around 632.8nm. This laser is used to track the position of the moving mirror.

Interferometer

The Vertex 80v spectrometer is equipped with an Ultra-Scan interferometer based on a linear scanner that produces highest possible spectral resolution (better than 0.07cm^{-1}).

The Fourier Transform Infrared Spectrometer is basically a Michelson interferometer. A beam splitter is used to split the beam from an internal light source into two beams. One beam path contains a movable mirror which introduces a wavelength-dependent modulation of the beam. The two beams reconstruct and interfere before arriving at the sample where a photocurrent is generated. The beams travel a different optical path length, which introduces a phase difference resulting in an interference pattern called an interferogram. The Fourier transform method is used to compute the photocurrent from the interferogram pattern.

The block diagram of vertex 80v *FTIR* spectrometer is shown below:

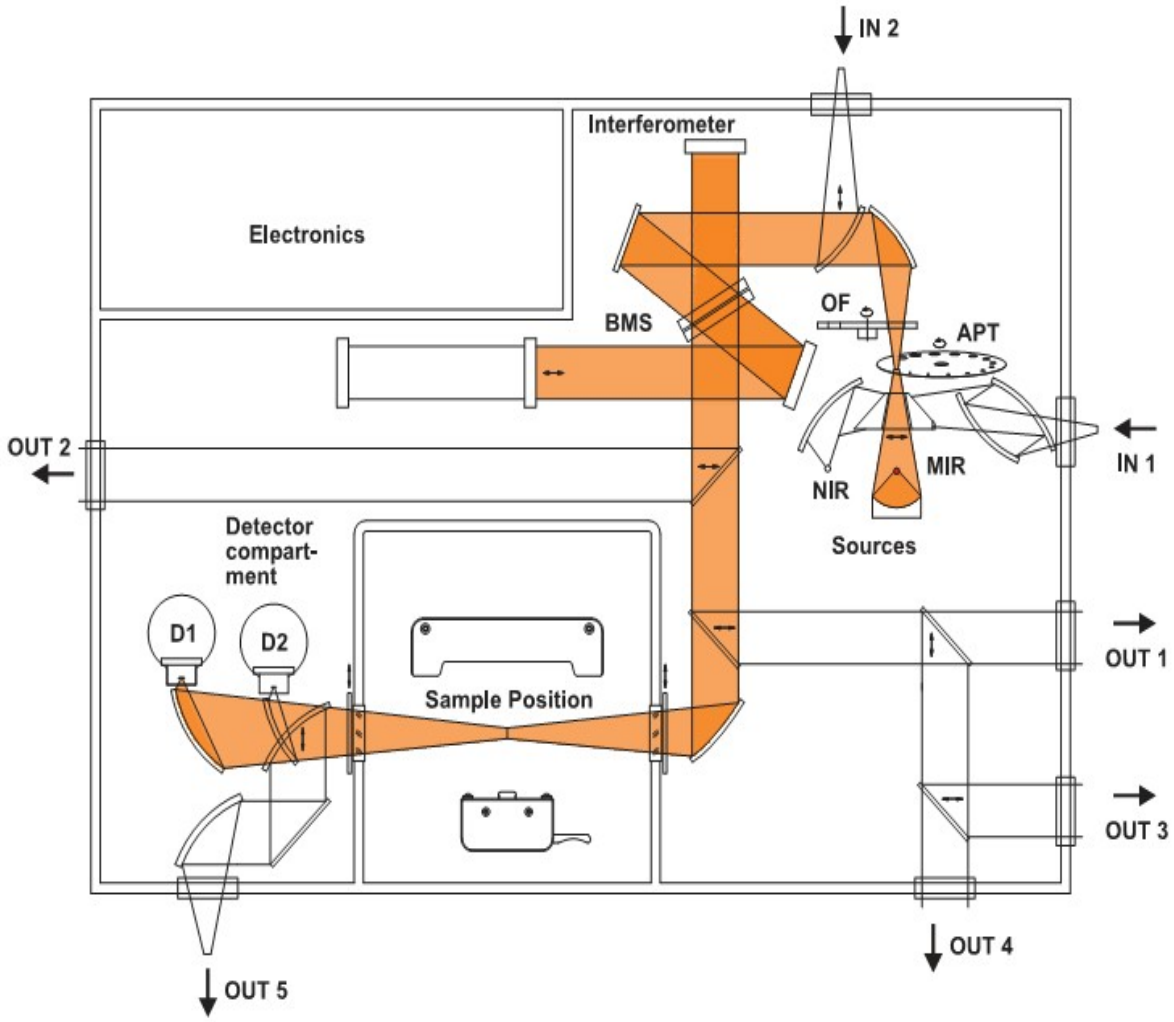

Figure 4.1: Block diagram of *FTIR* [15]

4.2) Cryostat:

The spectrometer is equipped with an integrated low vibration pulse tube (Model PT-950-FTIR) closed-cycle Helium cryostat. The temperature is variable between 5K and 300K [16].

Figure 4.2: Schematics of cryostat [16]

4.3) Keithley 6430 Source Meter

The Keithley 6430 source meter is used to record DC I-V measurements on devices. The data collection is done with the application software Lab Tracer. The source meter is directly connected to the sample rod where up to 7 two-terminal devices can be mounted and individually accessed from a switch box.

4.4) Keithley 428 Current Amplifier

The Keithley 428 current amplifier is used to measure and amplify the photocurrent generated by a photodetector under test and to convert it to a voltage. The measured photocurrent is modulated by the moving mirror in the interferometer. The spectrally resolved photocurrent is extracted by the spectrometer software (OPUS) using the Fourier transforms.

5 Results and Analysis

I-V Characteristics

I-V curves of two different devices are shown below. The area of device A5P & C3Q is about 800 * 800 and 200 * 200 in μm^2.

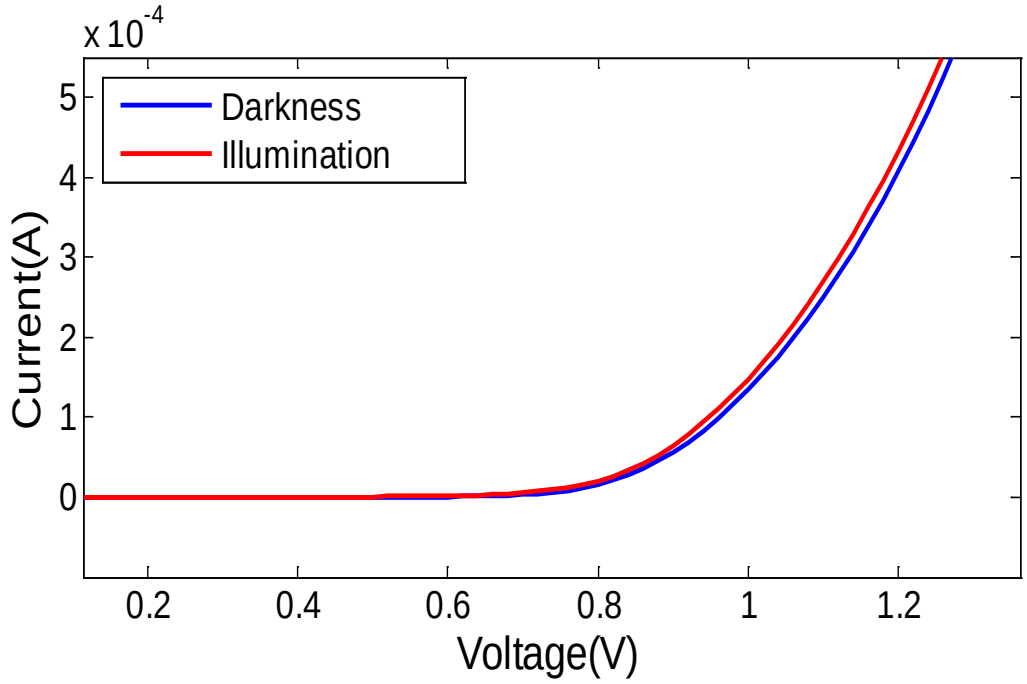

Graph 5.1: I-V curve of device A5P under darkness and illumination conditions in linear scale

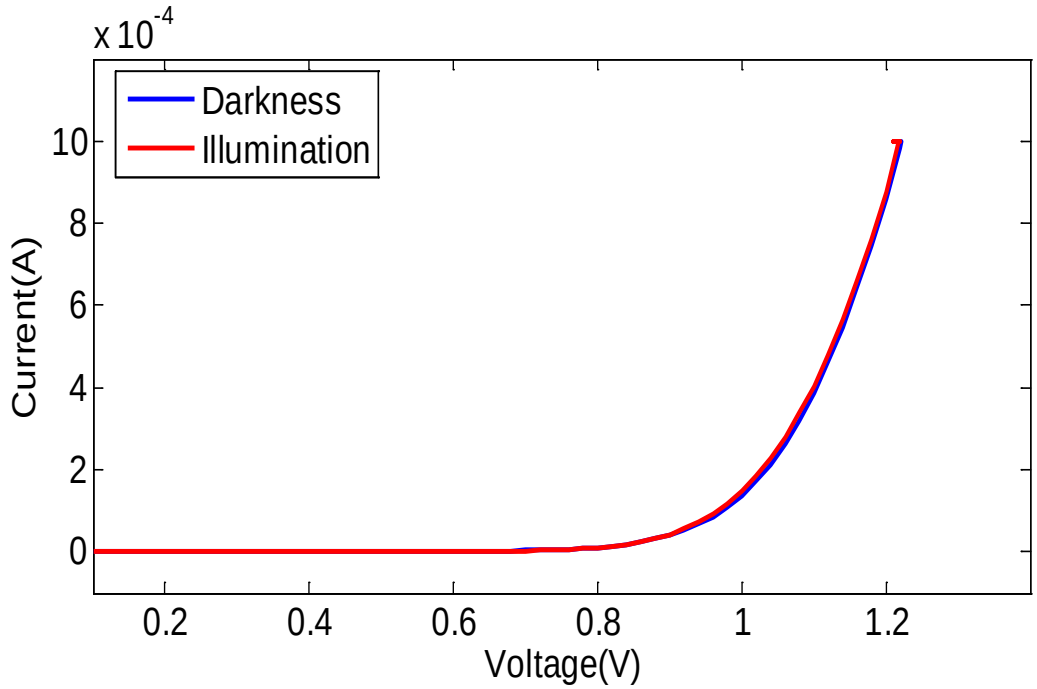

Graph 5.2: I-V curve of device C3Q under darkness and illumination conditions in linear scale. The graphs show that the onset voltage of devices is about +0.7V and +0.8V, respectively.

I-V curves of the devices are shown in semi-log scale. The included straight lines are linear fits to the dark forward current data points for extraction of the ideality factor.

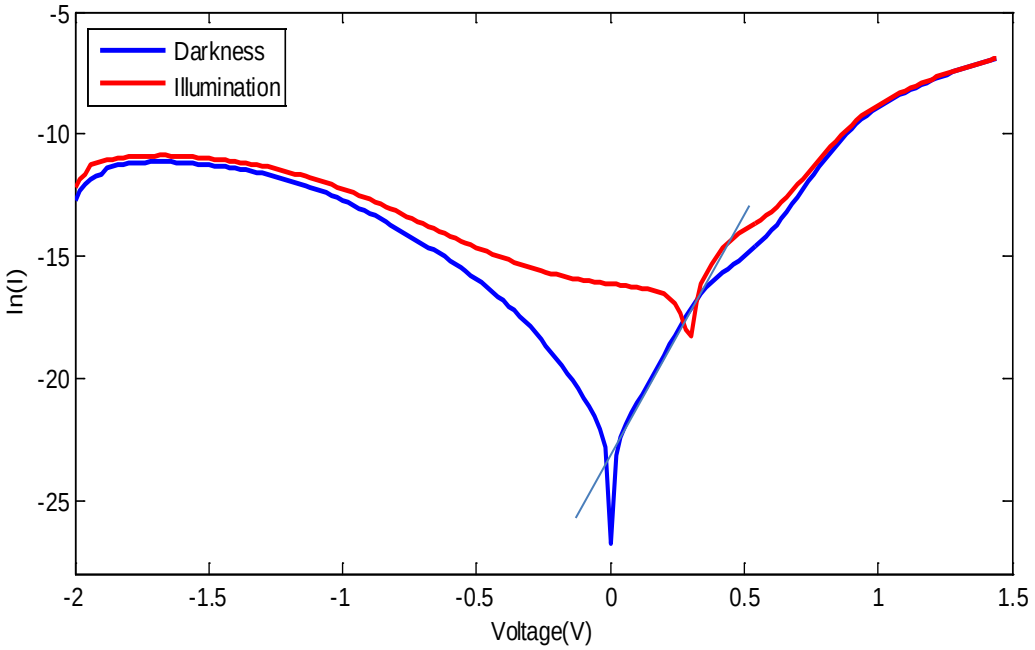

Graph 5.3: lnI versus voltage of device A5P under darkness and illumination conditions in semi-log scale

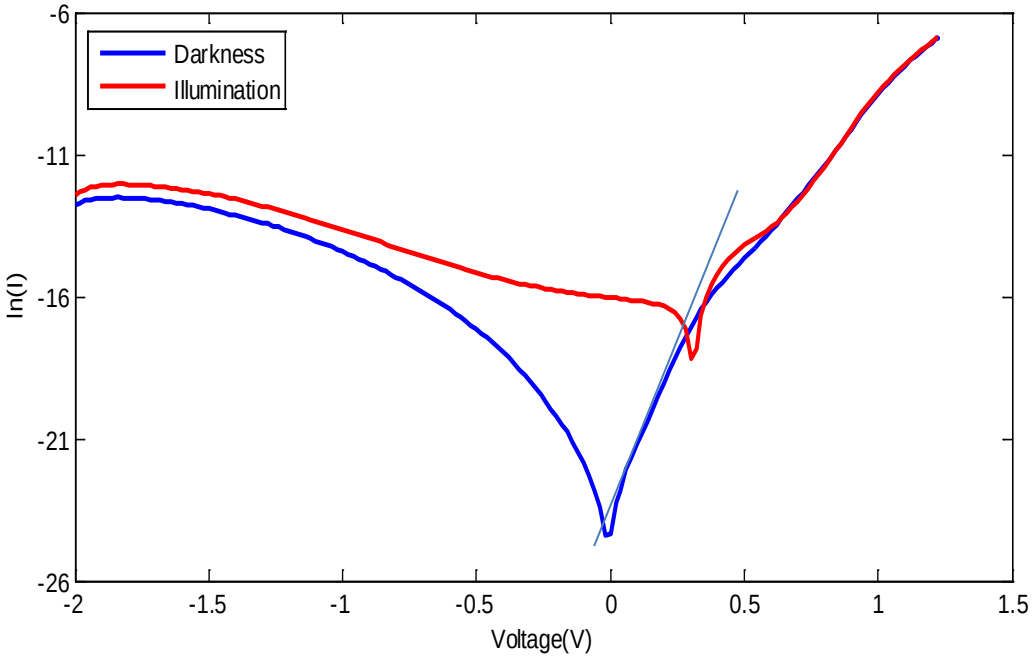

Graph 5.4: lnI versus voltage of device C3Q under darkness and illumination conditions in semi-log scale

During illumination the *I-V* curves of the devices are shifted upwards due to the photocurrent.

Discussions

The current-voltage characteristics show a reasonable exponential response under forward bias conditions. At high forward bias, the series resistance starts dominating the device performance and causes high internal resistance of the photodiode.

The current-voltage characteristics in reverse bias display a significant leakage current. One reason for this could be surface currents flowing on the NWs. Therefore, different surface passivation schemes should be tested in future experiments. For example, the surfaces of the NWs could be treated with an ammonium sulphate solution. Different insulator materials between the NWs could also be tried, e.g. replacing the silicon dioxide by silicon nitrate.

The ideality factor of both devices is around $\eta \approx 2$ at 300K, which indicates the recombination current.

Low-temperature measurements

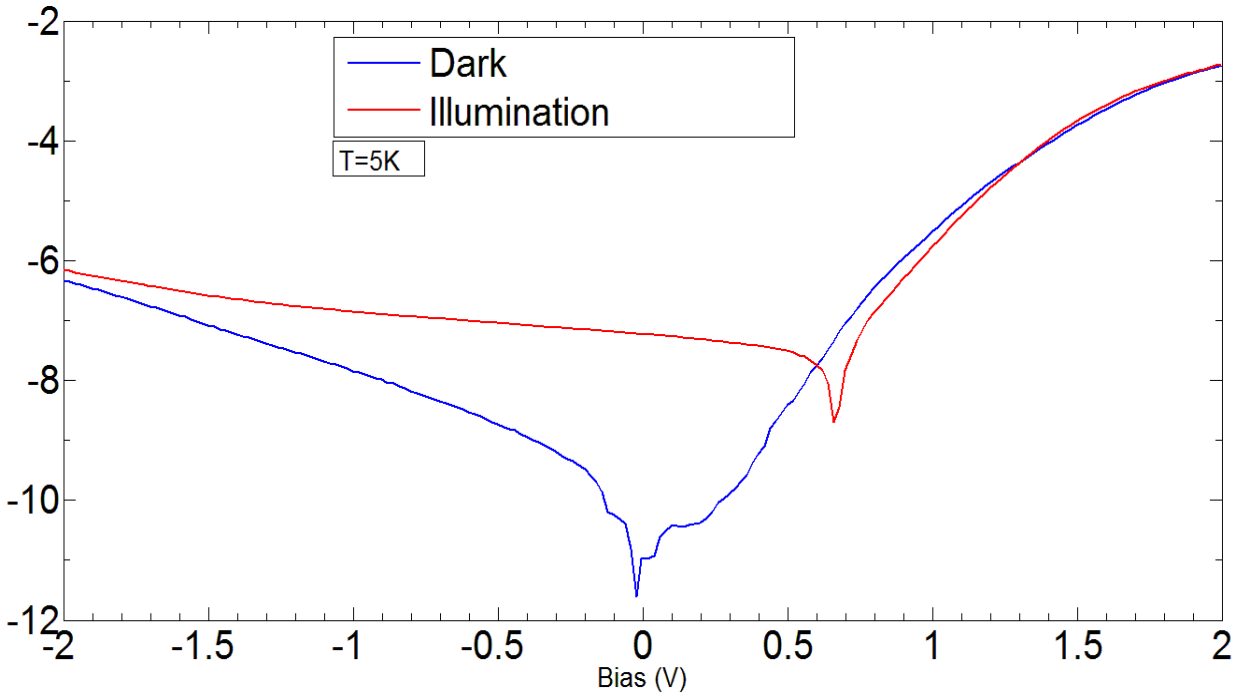

Graph 5.5: *I-V* curve of device C3Q at 5 K in semi-log scale

At low temperature, the dark current is decreased due to the reduction in thermal energy of electrons (i.e. kT).

Pure-photocurrent measurements

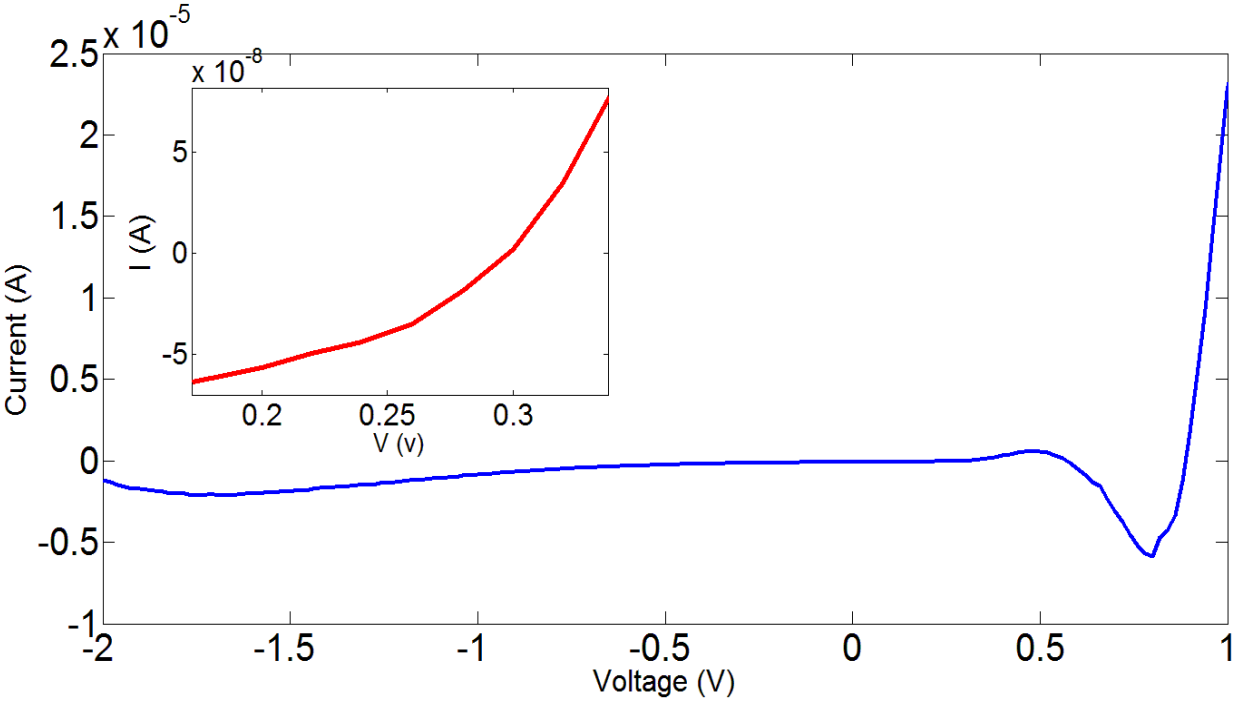

Graph 5.6: Pure photocurrent of device in linear scale

The blue curve shows the I-V of a photodiode under illumination. A clear rectifying behavior is observed as expected. The red curve represents pure photocurrent, which is total current minus dark current, with respect to applied bias. Initially the photocurrent is negative. At 0.3V the sign of the photocurrent is reversed, which we interpret as a strong contribution of photocurrent from the top segment of the nanowires. More specifically, we believe that a weak Schottky-like junction is formed between the moderately doped top segment in the nanowires and the ITO.

5.2) Optical characteristics

The photocurrent measurement of devices for different applied bias is shown below.

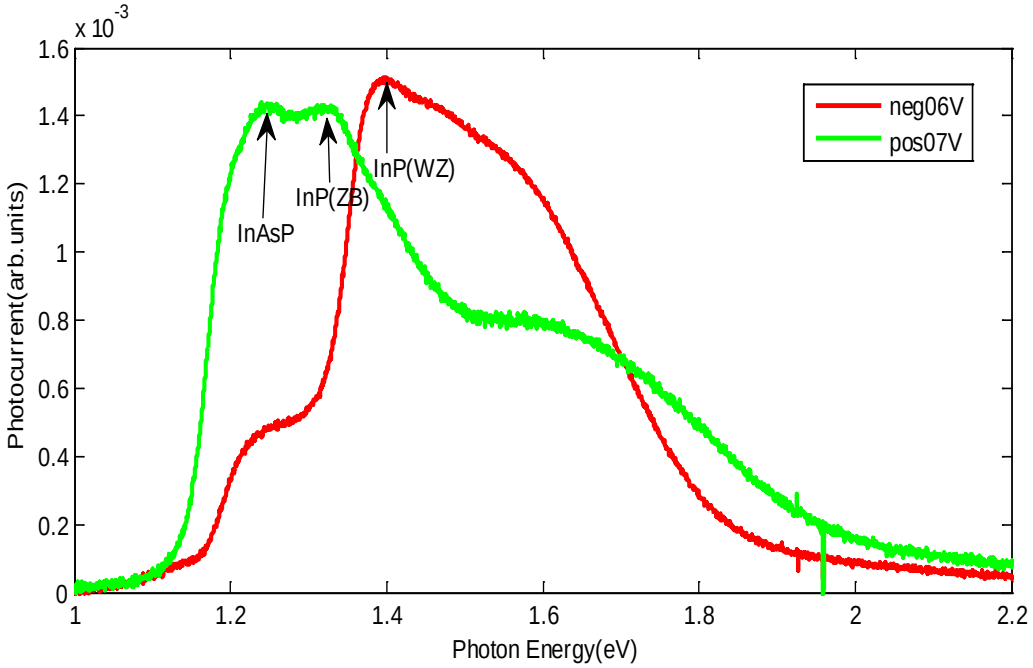

Graph 5.7: Photocurrent versus photon energy of device A5P

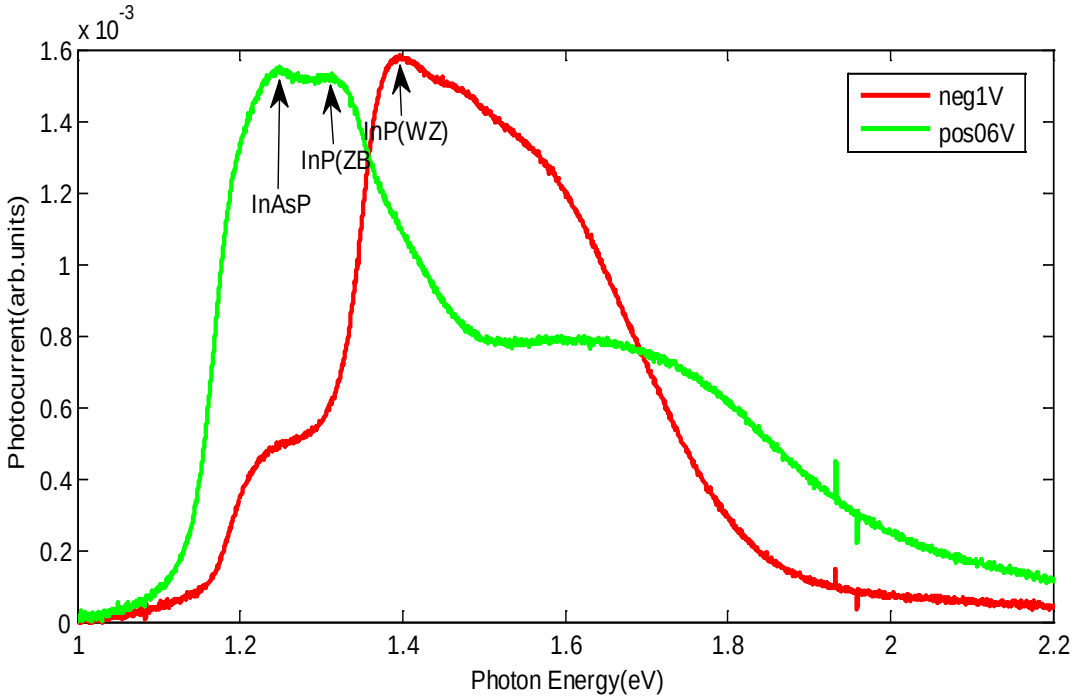

Graph 5.8: Photocurrent versus photon energy of device C3Q

Note:- Figures 5.7 and 5.8 show the spectrally resolved photocurrent for the two investigated samples at two different bias (0.6V reverse bias and 0.7V forward bias, respectively) at 300K.

Low-temperature measurements

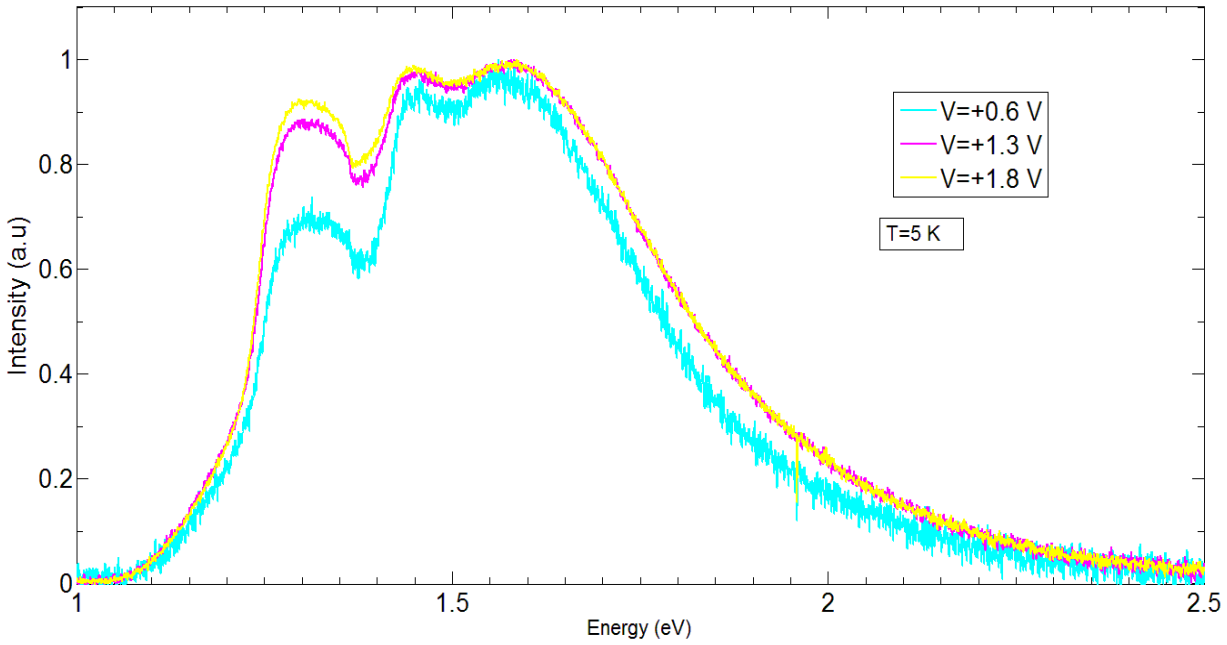

Graph 5.9: Photocurrent of device C3Q at 5K

From the graphs above we can draw some conclusions:

The dominant contribution to the photocurrent comes from inter-band transitions in the *InP* part of the NWs as seen in graph 5.7 & 5.8. Two different crystal phases exist in these NWs – wurtzite (WZ) and zinc blende (ZB). The bandgap of the wurtzite phase is about 80 meV larger than for the ZB phase [14]. The absorbed photons break the crystal bonds of *InP* and create free electron-hole pairs. The photo-generated charge carriers are swept away by the electric field thereby generating photocurrent. There is also a significant photocurrent generated in-between 1.1eV and 1.3eV as seen in graph 5.9. This photocurrent stems from inter-band transitions in the *InAsP* segment.

Schottky Current

The metal-semiconductor Schottky-like contacts form between the top n^+ InP segment of the nanowires and the sputtered indium tin oxide (ITO) layer. The depletion region is expected to be very shallow which explains a strong absorption and generation of photocurrent all higher photon energy (1.8eV - 2.5eV) as seen in figure 5.10. The effect of the Schottky diode could be minimized by increasing the doping concentration in the top segment of the nanowires.

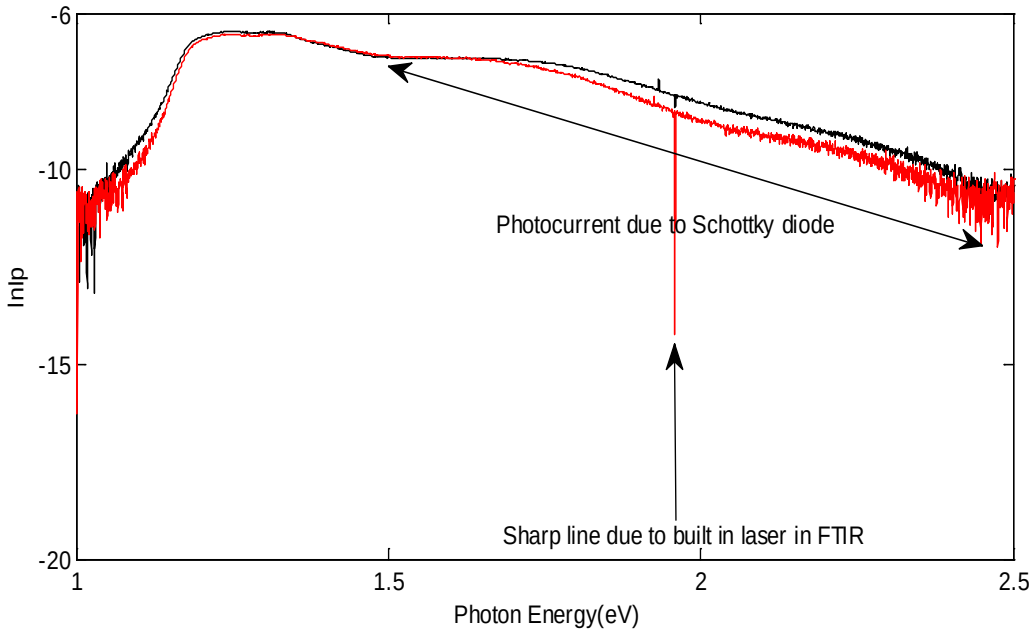

Graph 5.10: lnI versus photon energy of devices A5P (red curve) & C3Q (black curve) in semi-log scale

5.3) Breakdown Mechanisms

No clear reverse bias breakdown is observed for the NW-based array devices. To understand whether this absence stems from process-induced problems or fundamental problems with the grown NWs, single NW photodetectors were transferred onto insulating substrates and supplied with contacts using electron-beam lithography. Graph 5.11 below shows the breakdown measurements of a single NW photodetector in both linear and semi-log scale.

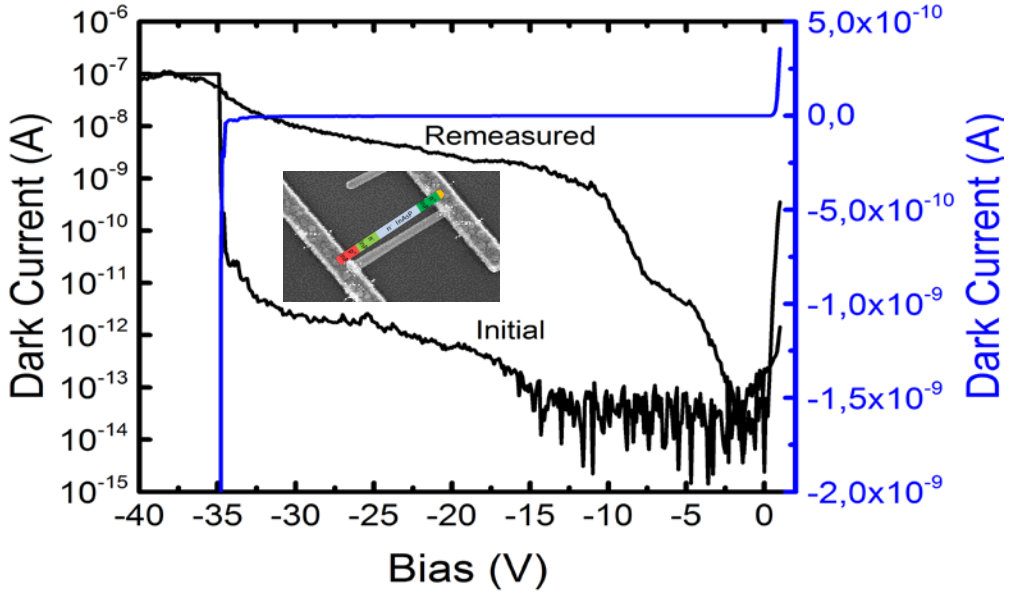

Graph 5.11: Dark current versus reverse bias voltage of single nanowire in both linear and semi-log scale

Clearly, an avalanche breakdown occurs at strong reverse bias around V_R=-35 volt in the pristine voltage sweep. The measurements were repeated after a few minutes and showed a strong degradation effect. This degradation effect is at present not understood. Detailed investigations, including surface passivation experiments, are presently carried out to investigate the underlying degradation mechanisms.

6) Conclusions

Optoelectronic properties of *InAsP/InP* NW-based avalanche photodetectors with separate absorption and multiplication regions have been studied with the help of Fourier transform infrared spectroscopy.

I-V characteristics of the devices show non-optimal diode response such as high dark current. Significant leakage currents flow in the detectors even in darkness indicating parasitic currents, possibly due to NW surface states. The extracted ideality factor of the devices for forward biased condition is $\eta \approx 2$. It shows reasonable exponential dependence under forward bias condition. Pure-photocurrent measurements conclude, photocurrents are generating from different segments of nanowire based on the bias voltage. No clear avalanche breakdown effect is observed for the array detectors. In single NW devices, a strong breakdown is observed at V_R=-35V in good agreement with theory.

The spectrally resolved photocurrent data agree well with transitions in both the InP and InAsP NW segments.

7 References

[1] S.M. Sze, "Semiconductor Devices Physics and Technology", 2nd Ed. John Wiley and Sons, Inc., (2002)

[2] Jagdeep shah, "Hot carriers in semiconductor nanostructures", Academic Press Inc., (1992)

[3] S.M. Sze and Kwok K. Ng, "Physics of semiconductor devices", 3rd Ed. John Wiley and Sons, Inc., (2007)

[4] Gunasekaran, Physics for higher secondary Vol.I, Vol. II, revised edition, Gov TN, (2007)

[5] David A.B. Miller, "Optical physics of quantum wells", At&T Bell Laboratories, Holmdel, Nj07733-3030

[6] By Hamamatsu Photonics, "Characteristics and uses of Silicon Avalanche photodiode", Solid state division, May (2004)

[7] Mark fox and Radu Ispasoiu, "Quantum well, Super lattices and Bandgap Engineering", Chapter 42 (2007)

[8] Farhan Rana, Semiconductor Optoelectronics, Cornell University, Chapter 2

[9] Maria Tchernycheva, George E. Cirlin, Gilles Patriarche, Laurent Travers, Valery Zwiller, Umberto Perinetti and Jean-Christophe Harmand, "Growth and Characterization of InP Nanowires with InAsP Insertions", ***Nano Lett.***, (2007), 7 (6), pp 1500–1504

[10] Chen Yang, Carl J. Barrelet, Federico Capasso, and Charles M. Lieber, "Single p-Type/i-Intrinsic/n-Type Silicon Nanowires as Nanoscale Avalanche Photodetectors", In **Nano Lett.,** (2006), 6, (12)

[11] Gabriele Bulgarini, Michael E. Reimer,Mo¨ıra Hocevar,Erik,P.A.M. Bakkers,, Leo P. Kouwenhoven and Valery Zwiller, " Avalanche amplification of a single exicition in a semiconductor Nanowire", **Nature Photonics**, 6,pp 455–458,(2012)

[12] Maria E. Messing, Karla Hillerich, Jonas Johansson, Knut Deppert and Kimberly A. Dick, "The use of gold for fabrication of nanowire structures", **Gold Bulletin**, 42, (3) pp 172-181, (2009)

[13] Jilang dawei, "Electrical and optical characteristics of InP nanowire based photodetectors", Halmstad University (2014)

[14] G.L. Tuin, "Optical characterization of wurtzite Indium Phosphide", Lund University (2010)

[15] Bruker Optics, VERTEX 80/80v FTIR user manual, August (2006)

[16] Janis, PT-950-FTIR model cryostat product overview, May (2015)

8 Appendixes

Appendix A

List of devices and their parameters:

i. Device-A5P

Area: 800 * 800 μm^2

ii. Device-C3Q

Area: 200 * 200 μm^2

Density of NWs on surface ≈ 6.3 per μm^2

Total NW length: 2 - 2.2 µm

n+ InP	n- InAsP	n InP	p+ InP
300-350 nm	1200-1400 nm	200-250 nm	200-250 nm

Doping Concentrations:

n^+ InP segment ≈ 6-10 * 10^{17} cm^{-3}

n^- InAsP segment ≈ 1-5 * 10^{15} cm^{-3}

n InP segment ≈ 1-5 * 10^{16} cm^{-3}

p^+ InP segment ≈ 5 * 10^{18} cm^{-3}

Appendix B

The graphs show a generated photocurrent with respective wavelength spectra.

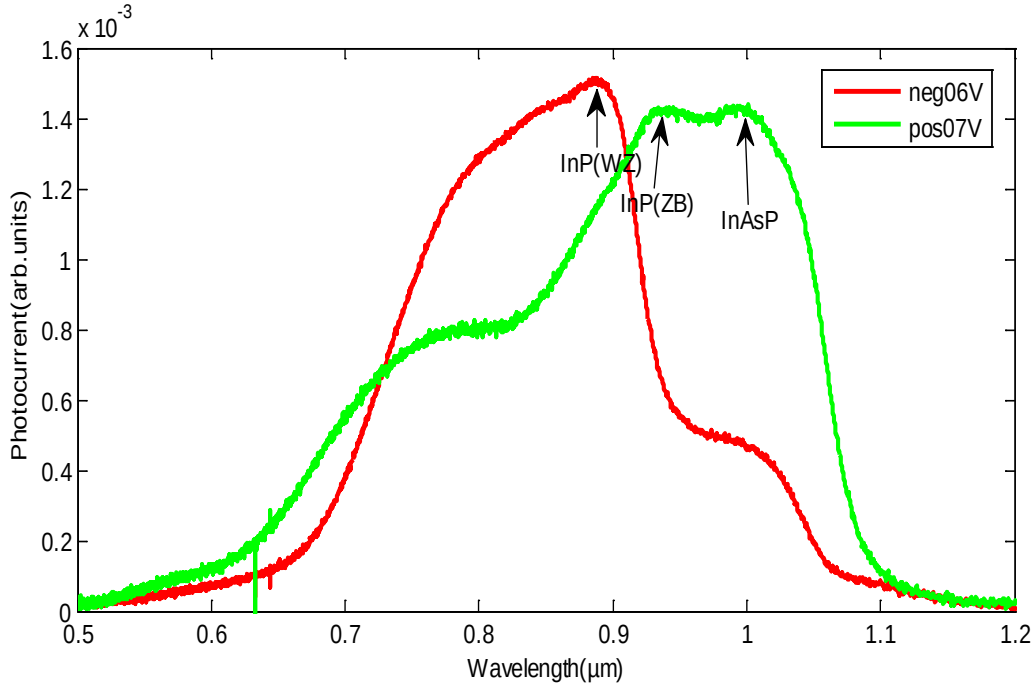

Device-A5P

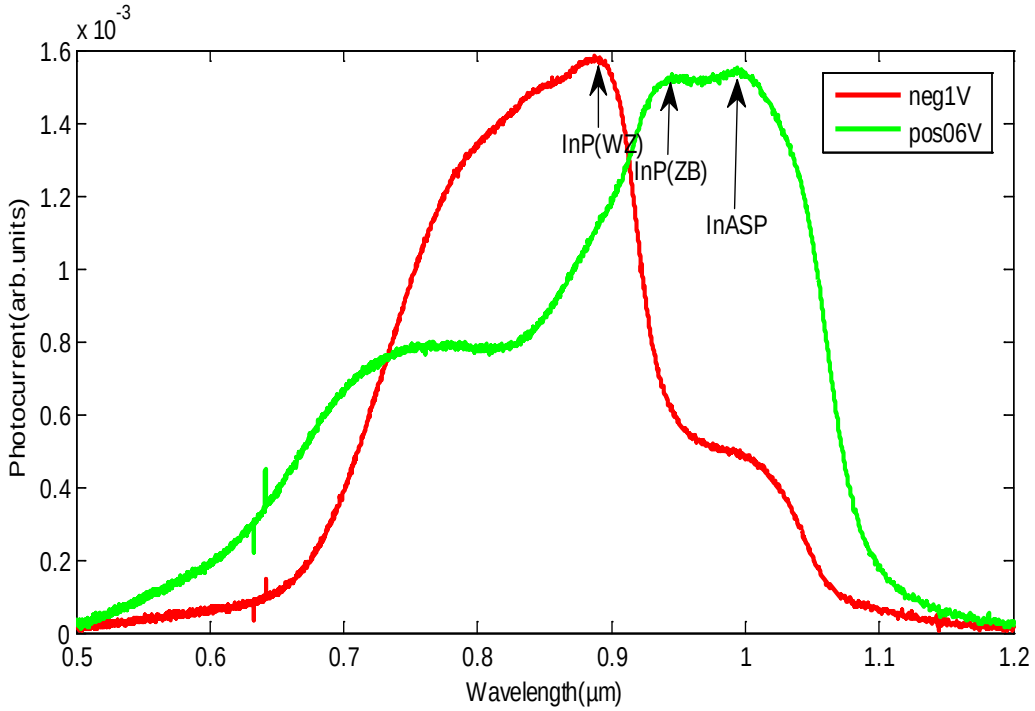

Device-C3Q

9 Laboratory Information

1) **Rydberg Laboratory** founded in 2004

Research facilities:
Physics, Microwave technology & Interferometry, Chemistry, Biology and Topography
Publications:
http://www.hh.se/english/schoolofbusinessengineeringandscience/research/rydberglaboratory/publications.3667.html
Co-ordinator:
Professor Håkan Pettersson
Halmstad University
Kristian IV väg 3
PO BOX 823
SE-301 18 Halmstad

2) **Nanometer Structure Consortium** founded in 1988

Research facilities:
Nano electronics & Nano photonics, Quantum Physics, Materials science, Nanobiology & Nano neuroscience, Nano energy and Nano safety
Publications:
http://www.nano.lu.se/tibet/template/personal,Index.vm?pageid=129468&siteid=1040
Co-ordinator:
Professor Lars Samuelson
Lund University
John Ericssons Väg 3
SE-221 00 Lund

Praveen Kumar Singaravelu
Mohammad Tawhidul Alam

PO Box 823, SE-301 18 Halmstad
Phone: +35 46 16 71 00
E-mail: registrator@hh.se
www.hh.se